Electronic Supplementary Information

Small pore black TiO$_2$/-large pore Fe$_3$O$_4$ cascade nanoreactor for chemdynamic/photothermal synergetic tumour therapy

Yali Shi,[a] Wenya Chang,[b] Liying Zhao,[a] Jiaqi Zhang,[a] Yumeng Yue,[a] Zhuoying Xie*[b] and Dawei Deng*[a]

[a] *Department of Biomedical Engineering, and Department of Pharmaceutical Engineering, School of Engineering, China Pharmaceutical University, Nanjing 211198, China. E-mail: dengdawei@cpu.edu.cn (D. Deng)*
[b] *State Key Laboratory of Bioelectronics, Southeast University, Nanjing 210096, China. E-mail: zyxie@seu.edu.cn (Z. Xie)*

* Corresponding Authors

Materials

All chemicals used in this work were analytical grade and used without further purification. Ferric chloride hexahydrate (FeCl$_3$·6H$_2$O, 99%),ethylene glycol (EG, 99%), sodium acrylate (CH$_2$=CHCOONa, Na acrylate), sodium acetate (CH$_3$COONa, NaOAc), diethylene glycol (DEG), Poly(vinylpyrrolidone) (PVP, K30), anhydrous ethanol, pluronic triblock copolymers poly(ethylene glycol)-block-poly(propylene glycol)-block-poly(ethylene glycol) (F127, average Mn~12600, PEO$_{106}$PPO$_{70}$PEO$_{106)}$, acitic acid (HOAc, 99%), tetrahydrofuran (THF, 99%), tetrabutyl titanate(TBOT, 99.5%), tetraethyl orthosilicate (TEOS, 98%), glycerol(99%), and lactate(LA) were purchased from Sigma-Aldrich Chemical. Concentrated hydrochloric acid (HCl, 28~30%), aqueous ammonia solution (NH$_3$·H$_2$O, 25%) was obtained from Sinopharm Group Chemical Reagent Co., Ltd. Lactate oxidase purchased from Yuan ye Biological Co., Ltd. trypsin (0.25%), DMEM/1640, MTT, Bradford assay kit, and 2',7-dichlorofluorescein diacetate (DCFH-DA) penicillin-streptomycin, and fetal bovine serum were purchased from Beyotime Biotechnology Co. Ltd. Annexin V-FITC/PI cell apoptosis detection kit, Live-dead cell stain assay kit, and JC-1 assay kit was purchased from KeyGEN Bio TECH (Jiangsu, China).

Characterizations

Transmission electron microscopy (TEM) images were taken using an HT7700 (Hitachi) or JEM-1200EX (JEOL) transmission electron microscope with an accelerating voltage of 100 kV. High-resolution TEM images (HRTEM) and EDS elemental mapping were taken on a JEM-2100F transmission electron microscope (JEOL) with an accelerating voltage of 200 kV. The SEM imaging was taken using FEI-Nova-NanoSEM450 electron microscope. The nitrogen adsorption/desorption measurement were obtained with TriStar II 3020 surface area and pore size analyzer. Dynamic light scattering (DLS) and Zeta potential were examined by Litesizer 500 particle size potentiometer instrument of Anton Paar. The UV-vis absorption spectra

were acquired on Shanghai Prism UV Fluorescence Spectrophotometer. The XRD patterns were recorded by Rigaku smartlab9 high-resolution XRD. The XPS survey spectrum were measured by ESCALAB 250Xi spectrometer. The Fourier transform infrared (FTIR) spectra were obtained using IRAffinity-1S spectrometer. A Shimadzu UV-3600 Plus or Shimadzu UV-2550 spectrophotometer was employed to obtain absorption spectra. The cell images were obtained by Zeiss LSM 800 confocal laser scanning microscopy (CLSM) or an inverted fluorescence microscope system (Nikon Ti–S). The cell survival rate was measured with a microplate reader (Thermo fisher 1510, USA).
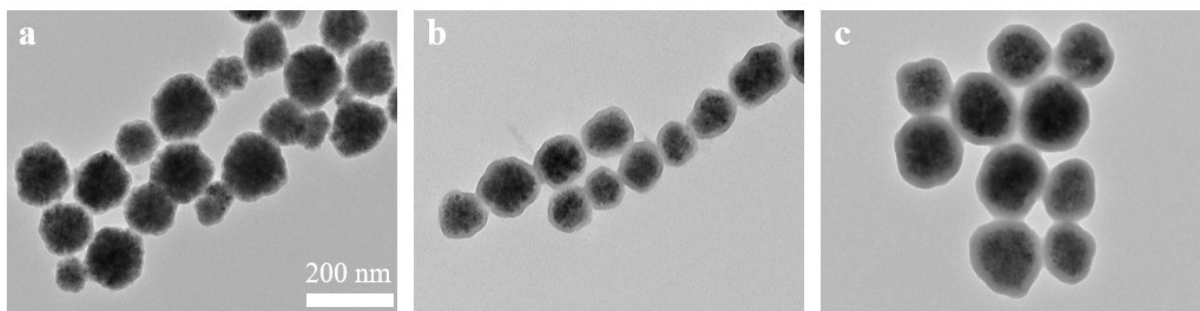
Fig. S1 The TEM images of Fe_3O_4 NPs coated with tunable thickness of SiO_2 shell: (a) 5 nm; (b) 10 nm; (c) 18 nm.
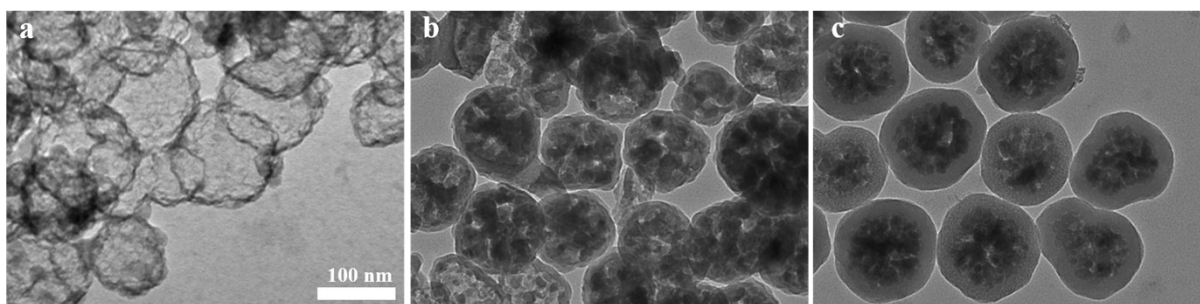
Fig. S2 TEM images of prepared $TiO_2/-Fe_3O_4$ NCs by using $SiO_2@Fe_3O_4$ NPs (Figure S1) with increased silicon layer thicknesses, showing various spatial strictures.

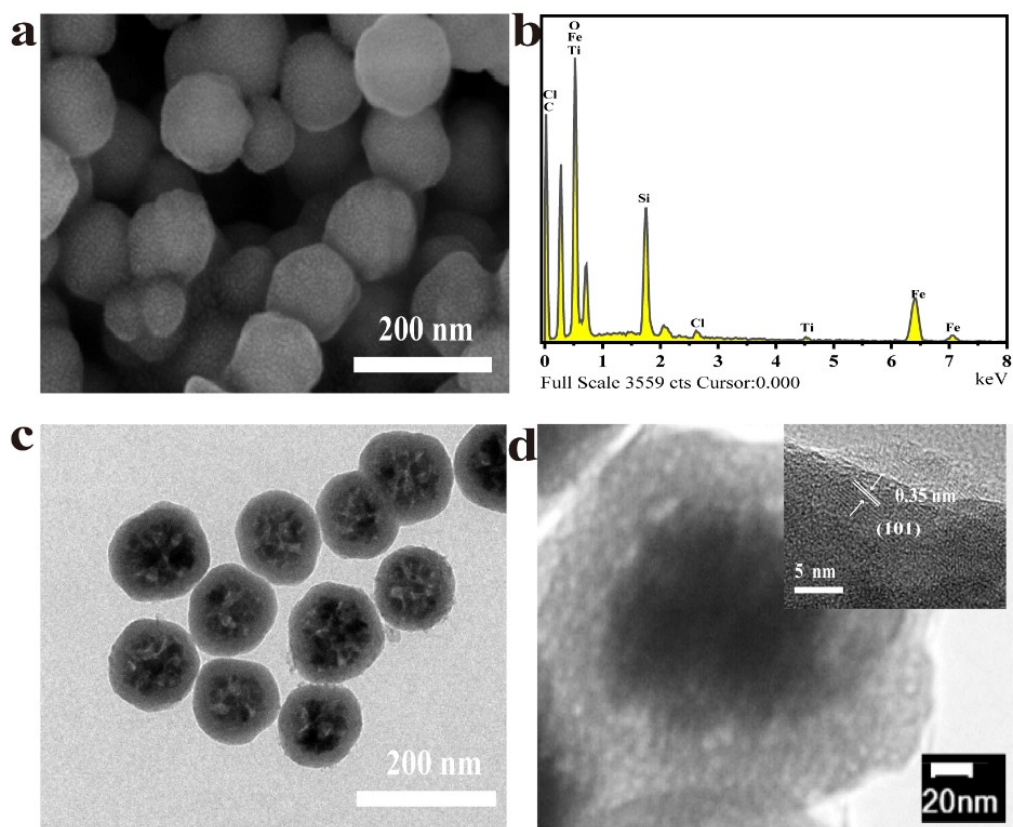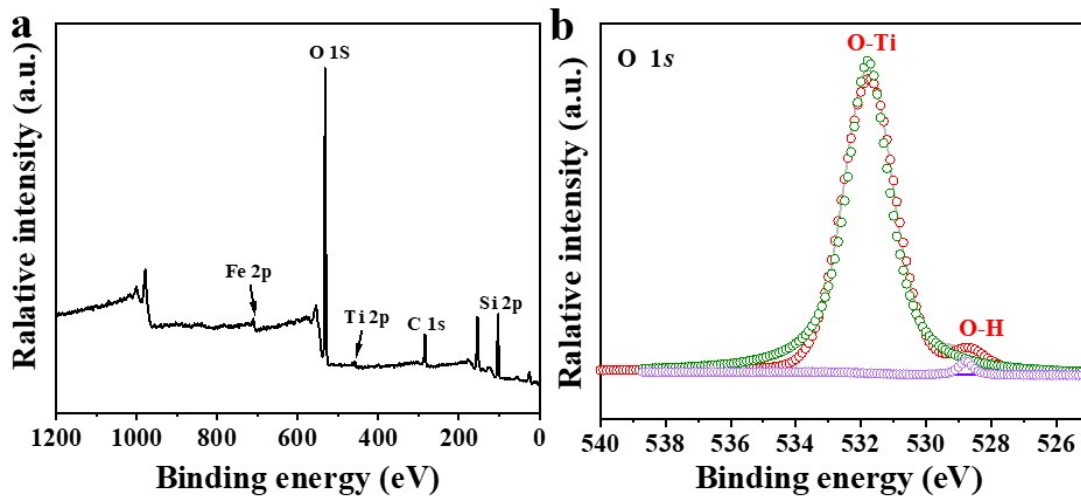Fig. S3 (a, b) The SEM image and EDS pattern of TiO$_2$/-Fe$_3$O$_4$ NCs. (c, d) TEM images and HR-TEM image (insert) of TiO$_2$/-Fe$_3$O$_4$ NCs.

Fig. S4 (a) XPS survey spectrum of $TiO_2/-Fe_3O_4$ NCs, showing the four characteristic bands of Fe, Ti, O, C and Si; (b) XPS high-resolution spectrum of O 1s.
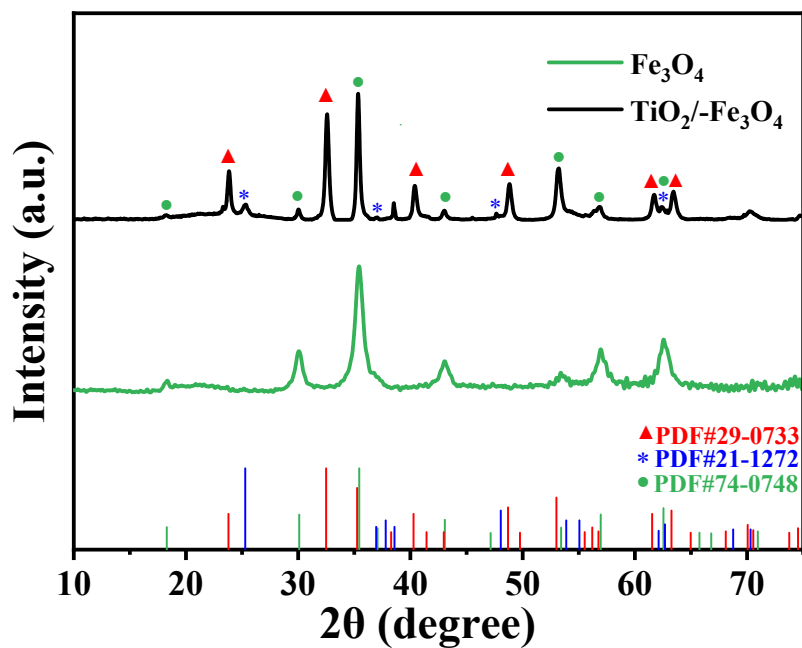

Fig. S5 XRD patterns of the resultant $TiO_2/-Fe_3O_4$ NCs and initial Fe_3O_4 NPs, compared to the standard anatase (space group I41/amd, JCPDS card No. 21-1272), magnetite (JCPDS card No. 74-0728), and $Fe^{2+}TiO_3$ (JCPDS card No. 29-0733).
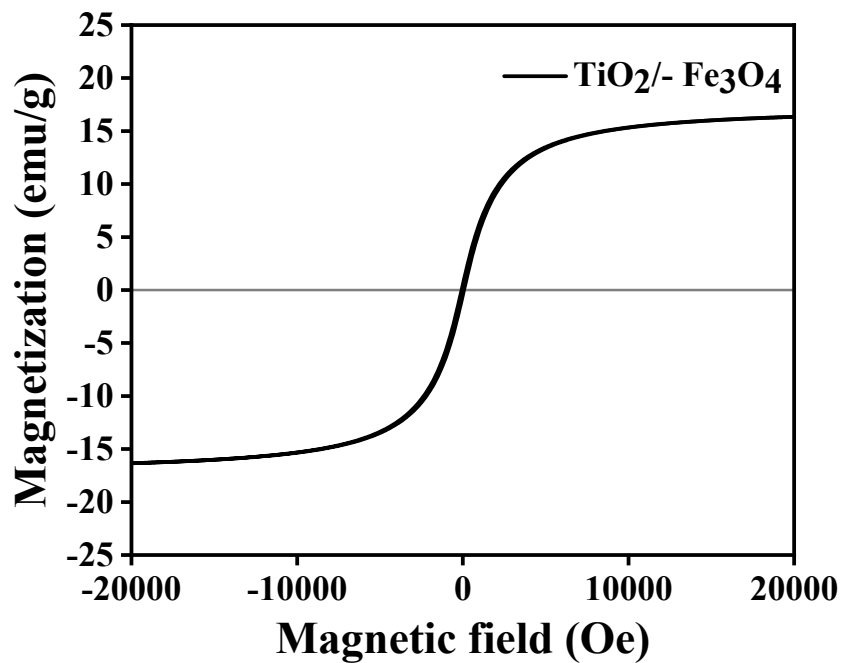
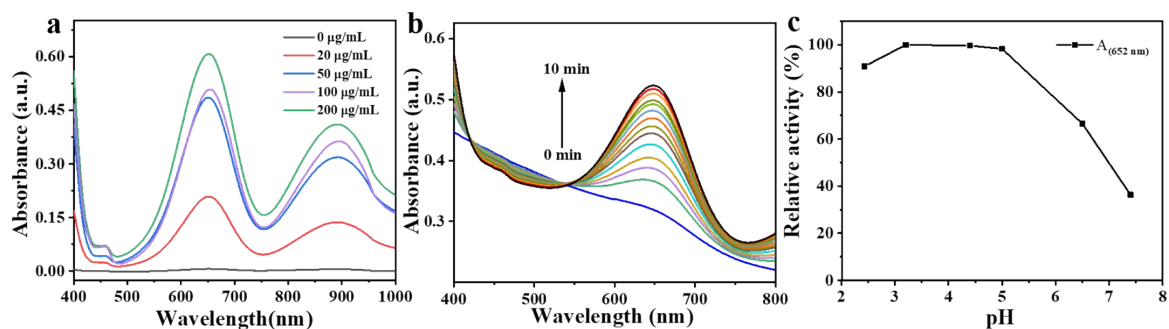Fig. S6 Magnetic hysteresis curve of $TiO_2/-Fe_3O_4$ NCs.

Fig. S7 The POD-like activity of $TiO_2/-Fe_3O_4$ nanozymes as a function of NCs concentration (a), incubation time (b), and pH (c). The maximum activity was set as 100%.
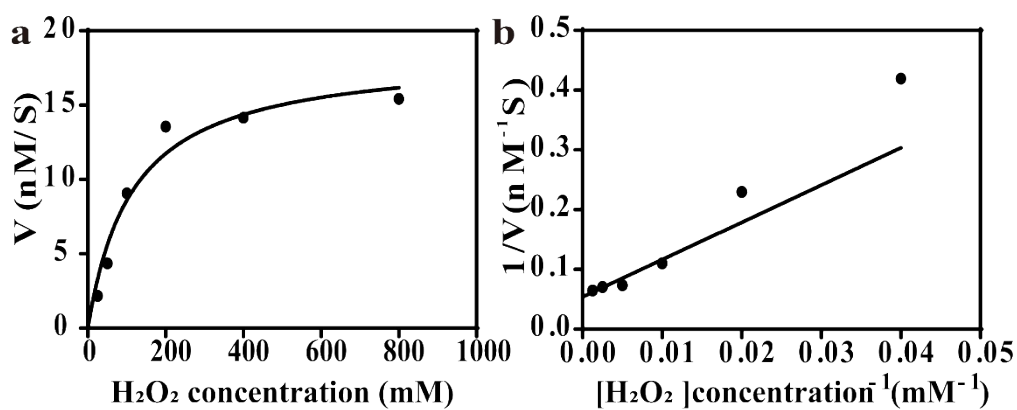

Fig. S8 The POD-like activity of Fe_3O_4 nanozymes. Michaelis-Menten kinetics (a) and Lineweaver-Burk plotting (b) of Fe_3O_4 nanozymes.
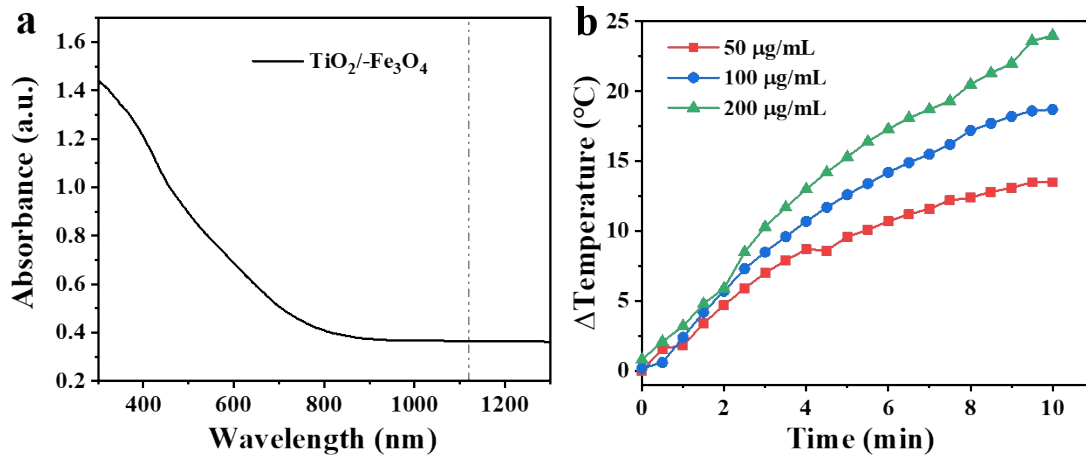
Fig. S9 (a) Ultraviolet-visible-NIR(UV-vis-NIR) absorption spectrum of $TiO_2/-Fe_3O_4$ solution. (b) Temperature variations of the different concentrations $TiO_2/-Fe_3O_4$ solution under irradiation by the 1120 nm laser at 1W.

The calculation equation of photothermal conversion efficiency was based on previous reports according to the eq1[1].

$$\eta = \frac{hs\,(Tmax - Tsur)\, - Q}{I(1 - 10^{-A_{1120}})} \tag{1}$$

The Tmax (K) is the equilibrium temperature; Tsurr (K) means ambient temperature of the surroundings. The Q (W) is heating loss from light absorbed by the container, and it is calculated to be approximately equal to 0 mW. I ($W \cdot cm^{-2}$) represents incident laser power density; A_{1120} is the absorbance of samples at 1120 nm. Where h ($W \cdot cm^{-2} \cdot K^{-1}$) means heat transfer coefficient, S (cm^2) represents the surface area of the container, the hS was calculated from the Figure 2g. The hS is calculated using the following eq 2

$$\tau_S = \frac{m_D C_D}{hs} \tag{2}$$

Where τs is the sample system time constant, m_D and c_D are the mass (1 g) and heat capacity (4.2 $J \cdot g^{-1} \cdot °C^{-1}$) of the solvent. Thus, according to calculating, the heat conversion efficiency (η) of the samples is listed in the Table S2.
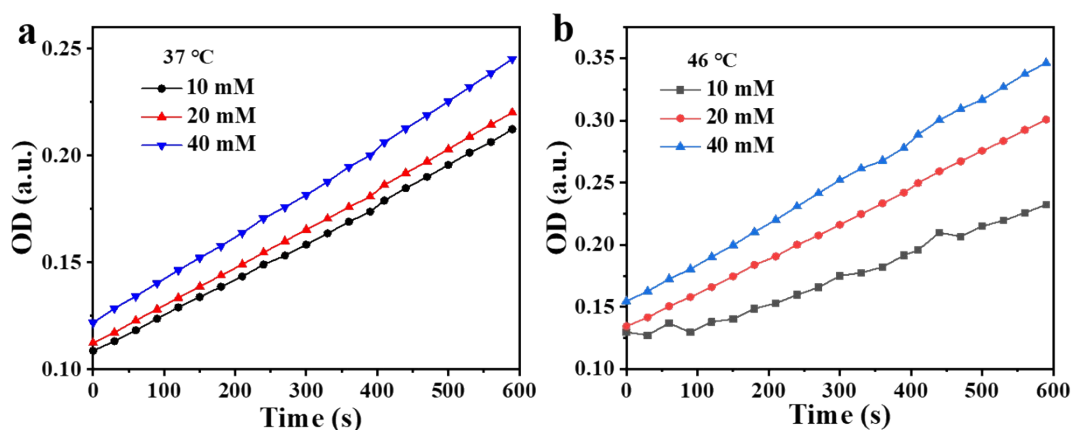
Fig. S10 Absorbance changes at 652 nm of TMB solution when $TiO_2/-Fe_3O_4$ nanozymes were incubated with different concentrations of H_2O_2 at 10, 20, and 40 mM at 37 ° C (a) and 46 ° C (b), respectively;
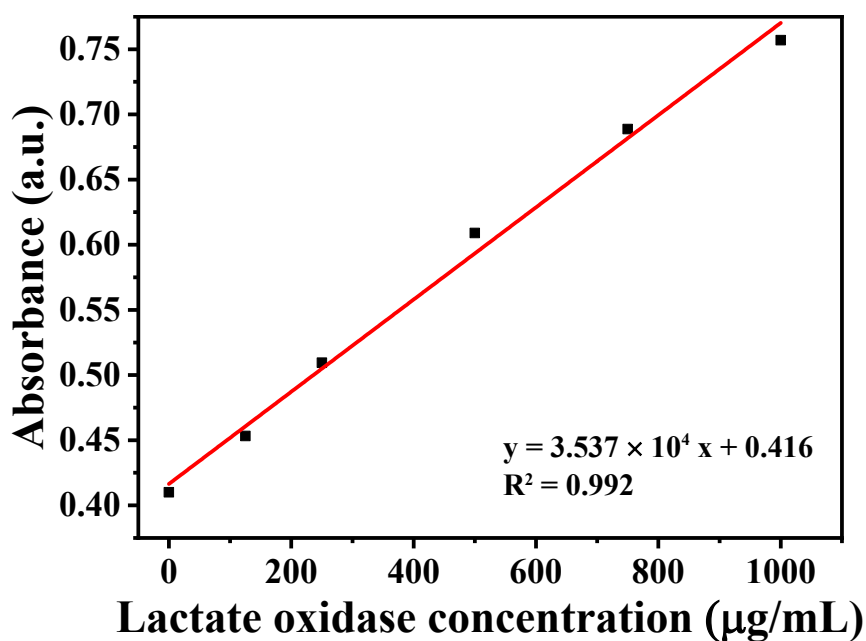

Fig. S11 The standard curve of absorption intensity of lactate oxidase a function of concentration. The absorption intensity was measured at 595 nm via the Bradford assay kit.
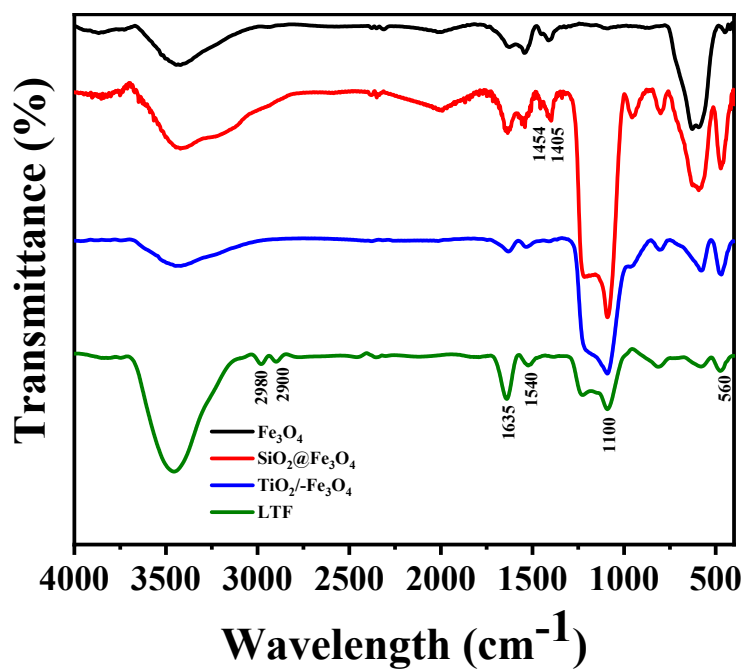
Fig. S12 FTIR spectra of the Fe_3O_4 NPs, $SiO_2@Fe_3O_4$ NPs, $TiO_2/-Fe_3O_4$ NCs, and LTF NCs. The peak at 1405 and 1540 cm^{-1} was the characteristic peak of carboxylate, and the characteristic peak at 1405 and 1540 cm^{-1} disappeared after calcination of $TiO_2/-Fe_3O_4$ NCs, indicating that the ligand PAA in Fe_3O_4 was decomposed, which was also the reason why the inner core Fe_3O_4 formed mesopores
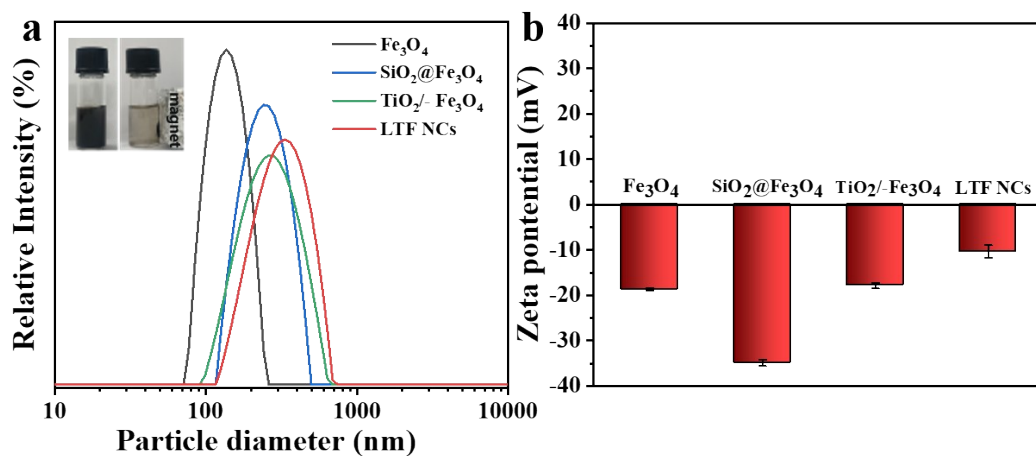
Fig. S13 (a, b) Hydration particle size distribution and the corresponding Zeta potential of Fe$_3$O$_4$ NPs, SiO$_2$@Fe$_3$O$_4$ NPs, TiO$_2$/-Fe$_3$O$_4$ NCs, and LTF NCs. Insert photograph of LTF NCs water solution.
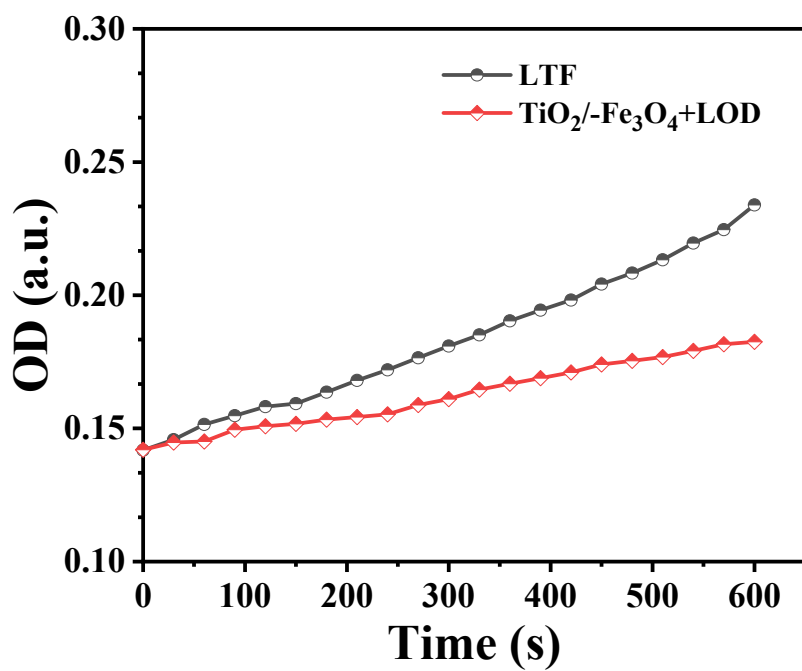
Fig. S14 The comparison of the catalytic performances of LOD immobilized at surface of $TiO_2/-Fe_3O_4$ NCs with free LOD.
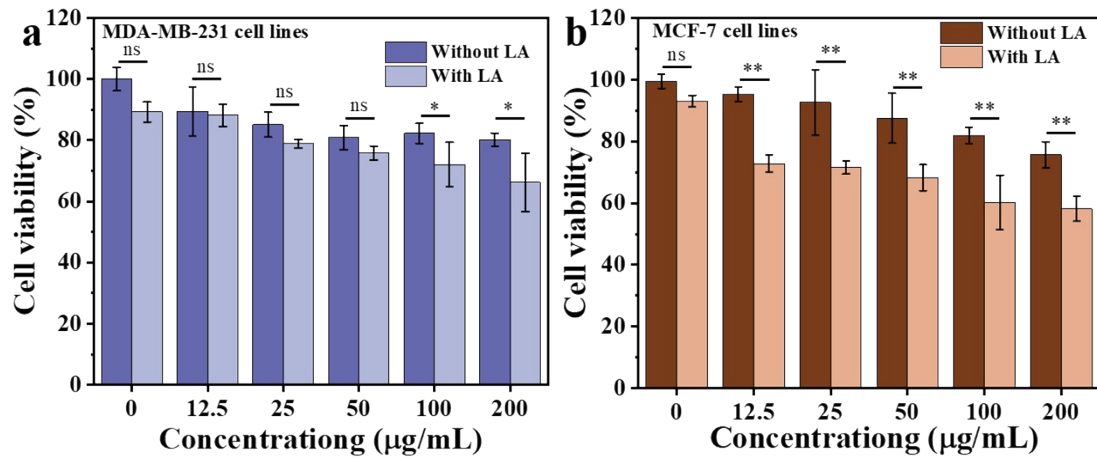
Fig. S15 Cell viability of MDA-MB-231 cells (a) and MCF-7 cells (b) incubated with LTF NCs with or without lactate. The data are presented as mean ± standard deviation (SD) (n = 3) with *P< 0.05, **P < 0.01, ***P < 0.001.
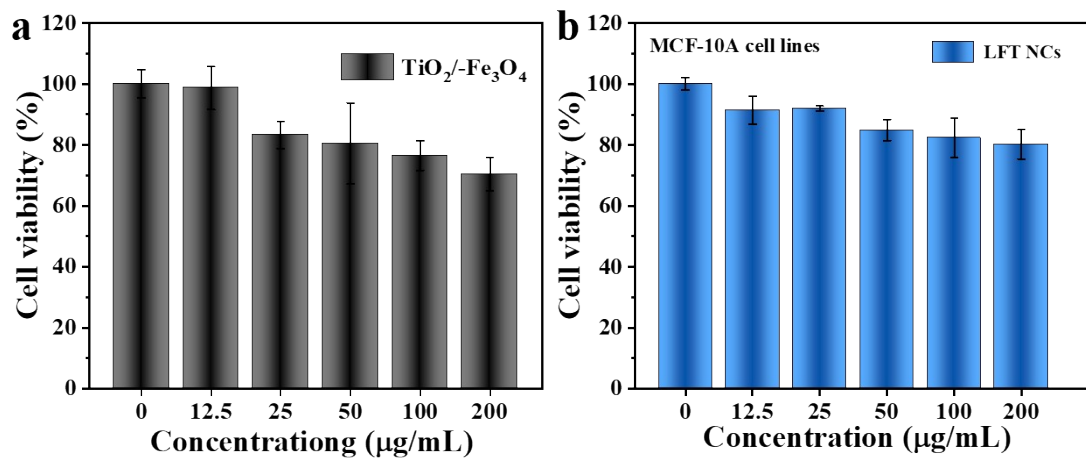

Fig. S16 (a) 4T1 cell viabilities incubation with different concentrations of $TiO_2/-Fe_3O_4$ NCs. (b) MCF-10A cell viabilities incubation with different concentrations of LTF NCs.
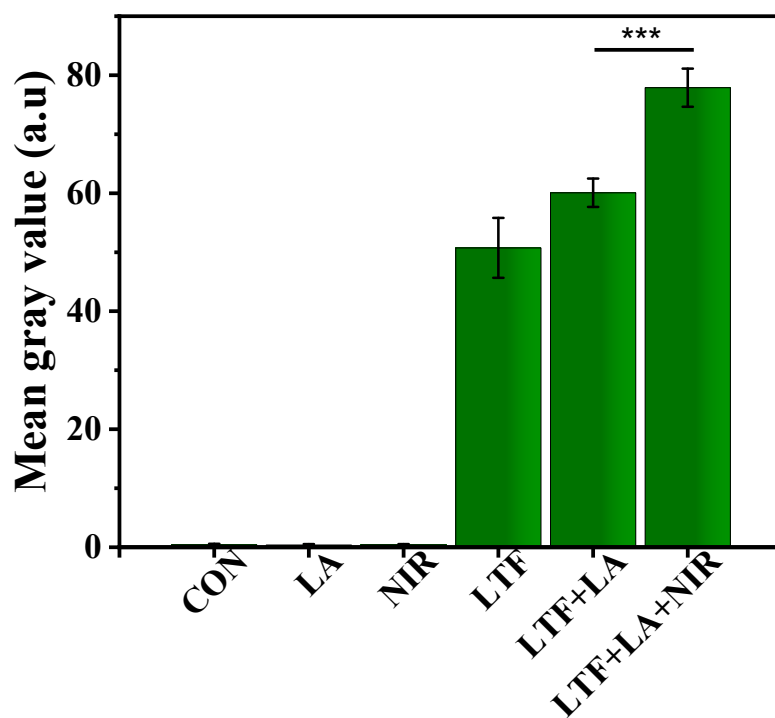
Fig. S17 Mean gray value of intracellular ROS levels of 4T1 cells under various treatments with LA (20 mM) corresponds to Figure 4a. The data are presented as mean ± standard deviation (SD) (n = 3) with ***P < 0.001.
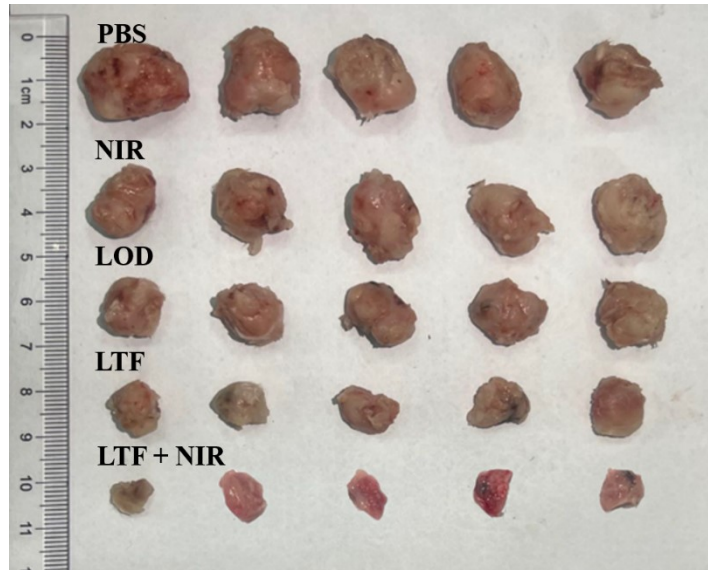
Fig. S18 Photographs of dissected tumors from 4T1 tumor-bearing mice in different treatment groups for 15 days.

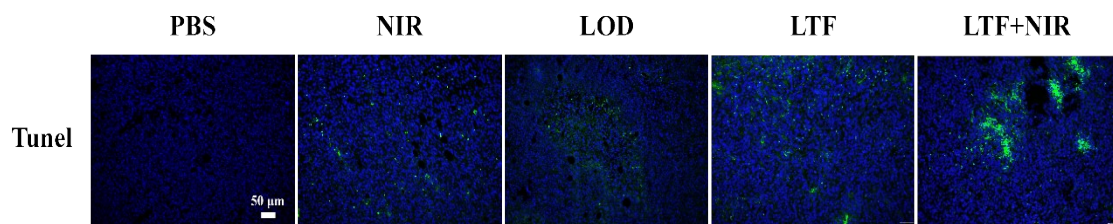
Fig. S19 Tunel staining for tumor tissues from 4T1 tumor-bearing mice after various treatments for 15 days (Scale bar: 50 μm).

Table S1. Kinetic parameters for the POD-like activity of Fe_3O_4 nanozymes, TiO_2/-Fe_3O_4 nanozymes and HRP with H_2O_2 as substrate. Km is the Michaelis constant, Vmax is the maximal reaction velocity.

	Km (mM)	Vmax (nM/S)
Fe_3O_4	115.30	18.50
Fe_3O_4-/TiO_2	6.06	18.81
HRP [2]	10.35	0.689

Table S2. The results calculation of photothermal conversion efficiency of TiO_2/-Fe_3O_4

	Tmax-Tsur	τ_S	A_{1120}	η
TiO_2/-Fe_3O_4	23.2	409.6	0.364	41.9 %

References

1. D. K. Roper, W. Ahn and M. Hoepfner, *J. Phys. Chem. C*, 2007, **111**, 3636-3641.

2. K. L. Fan, H. Wang, J. Q. Xi, Q. Liu, X. Q. Meng, D. M. Duan, L. Z. Gao and X. Y. Yan, *Chem. Commun.*, 2017, **53**, 424-427.